Efficient Regularized Field Map Estimation in 3D Parallel MRI

Claire Yilin Lin and Jeffrey A. Fessler

***Abstract*—Magnetic field inhomogeneity estimation is important in some types of magnetic resonance imaging (MRI), including field-corrected reconstruction for fast MRI with long readout times, and chemical shift based water-fat imaging. Regularized field map estimation methods that account for phase wrapping and noise involve nonconvex cost functions that require iterative algorithms. Most existing minimization techniques were designed for single-coil MRI, and are computationally or memory intensive for 3D datasets. This paper considers 3D MRI with coil sensitivity, and addresses the field map estimation problem in water-fat imaging. Our efficient algorithm uses a preconditioned nonlinear conjugate gradient method based on an incomplete Cholesky factorization of the Hessian of the cost function, along with a monotonic line search. Numerical experiments show the computational advantage of the proposed algorithm over state-of-the-art methods with similar memory requirements.**

***Index Terms*—Magnetic field inhomogeneity, field map estimation, water-fat imaging, preconditioned conjugate gradient, monotonic line search, incomplete Cholesky factorization**

I. Introduction

In magnetic resonance imaging (MRI), scans with long readout times require correction for magnetic field inhomogeneity during reconstruction to avoid artifacts [1]-[5]. Field inhomogeneity is also a nuisance parameter in chemical shift based water-fat imaging techniques [6]-[11]. Field map estimation is thus crucial to field-corrected MR image reconstruction, and for fat and water image separation.

One approach is to acquire MR scans at multiple echo times, usually with short readouts, and use the reconstructed images to estimate field inhomogeneity. Since field maps tend to be smooth within tissue, estimation methods with smoothness assumptions have been proposed, including region growing techniques [12]-[17], filtering [18], curve fitting [19]-[21], multiresolution and subspace approaches [14],[21]-[23], and graph cut algorithms [24]. Most of these methods, however, use various approximations to account for phase wrapping between different acquisitions. As an alternative, regularized estimation methods [5],[8]-[10] have been proposed to account for both phase wrapping and the smoothness of the field map from multiple acquisition images. Because the field map affects image phase, these approaches involve a nonconvex optimization problem that requires iterative methods.

This work was supported in part by NIH grants R01 EB023618, U01 EB026977, R21 AG061839, and NSF grant IIS 1838179.

C. Y. Lin is with the Department of Mathematics, University of Michigan, Ann Arbor, MI, 48109 USA (e-mail: yilinlin@umich.edu).

J. A. Fessler is with the Department of Electrical Engineering and Computer Science, University of Michigan, Ann Arbor, MI 48109 USA (e-mail: fessler@umich.edu).

To solve such optimization problems, [5],[9],[25] use a majorize-minimization (MM) approach by introducing a quadratic majorizer for their cost functions. The MM approach decreases the cost monotonically, but is computationally intensive, especially for large-scale datasets. Other regularized field map estimation minimization techniques quantize the solution space [8],[10] and may require a second descent algorithm to produce sufficiently smooth estimates. An alternative minimization technique [26] uses nonlinear conjugate gradient (NCG) with a monotonic line search (MLS), and explores its efficiency with various preconditioners in the 3D single-coil case.

This paper considers the regularized field map estimation problem in the 3D parallel MRI setting. In particular, we introduce a generalized cost function in the multi-coil case for both multi-echo field map estimation and water-fat imaging. We minimize it by a NCG algorithm with an efficient MLS and an iteration-dependent preconditioner based on an incomplete Cholesky factorization [27] of the Hessian of the cost function. In addition to faster convergence, this preconditioner exploits the sparse structure of the Hessian, thus it is memory efficient and scales to 3D datasets. Compared to previous works [9],[25],[26], our new approach unifies the field map estimation and the water-fat imaging problems, with a generalized expression that considers multiple coils in MRI. Our efficient algorithm on this problem shows significant computational and storage advantages compared with existing MM and NCG methods.

The rest of this paper is organized as follows. Section II introduces the optimization problem for the field map estimation problems for parallel MRI. Section III presents the NCG-MLS optimization scheme with the proposed preconditioner. Section IV reports simulated and real experimental results, followed by conclusions in Section V.

II. Problem Formulation

We are given reconstructed images $\boldsymbol{y}_{cl} \in \mathbb{C}^{N_\mathrm{v}}$ for the cth receiver coil of the lth scan, with $c = 1, \dots, N_\mathrm{c}$, $l = 1, \dots, L$, where N_v denotes the total number of voxels in the image, N_c denotes the number of coils, and L denotes the number of echo times. We model the field inhomogeneity effect as

$$y_{clj} = e^{i\omega_j t_l} s_{cj} x_{lj} + \epsilon_{clj}\,, \tag{1}$$

where $j = 1, \dots, N_\mathrm{v}$ is the voxel index, $\boldsymbol{\omega} \in \mathbb{R}^{N_\mathrm{v}}$ is the unknown field map, $t_l \in \mathbb{R}$ is the echo time shift of the lth scan, $\boldsymbol{s}_c \in \mathbb{C}^{N_\mathrm{v}}$ is the (known) coil sensitivity map for the cth

coil, and $\boldsymbol{\epsilon}_{cl} \in \mathbb{C}^{N_\mathrm{v}}$ denotes the noise. The unknown image $\boldsymbol{x}_l \in \mathbb{C}^{N_\mathrm{v}}$ for the lth echo is problem-dependent, where

$$x_{lj} = \begin{cases} m_j & \text{in field map estimation,} \\ m_{\mathrm{w},j} + m_{\mathrm{f},j} e^{i2\pi\Delta_\mathrm{f} t_l} & \text{in water-fat imaging,} \end{cases}$$

where $\boldsymbol{m}, \boldsymbol{m}_\mathrm{w}, \boldsymbol{m}_\mathrm{f} \in \mathbb{C}^{N_\mathrm{v}}$ are respectively the magnetization, water, and fat components, and $\Delta_\mathrm{f} \in \mathbb{R}$ denotes the (known) chemical shift of fat. The goal of the field map estimation problem is to estimate $\boldsymbol{\omega}$ and $\boldsymbol{x}$ given $\boldsymbol{y}$ and $\boldsymbol{s}$.

Assuming the noise $\boldsymbol{\epsilon}$ is zero-mean, white complex Gaussian, the joint maximum-likelihood (ML) estimates of the field map $\boldsymbol{\omega}$ and image $\boldsymbol{x}$ are given by

$$\underset{\boldsymbol{\omega},\boldsymbol{x}}{\operatorname{argmin}} \widetilde{\Phi}(\boldsymbol{\omega}, \boldsymbol{x}), \text{ where}$$

$$\widetilde{\Phi}(\boldsymbol{\omega}, \boldsymbol{x}) = \sum_{j=1}^{N_\mathrm{v}} \sum_{l=1}^{L} \sum_{c=1}^{N_\mathrm{c}} |y_{clj} - e^{i\omega_j t_l} s_{cj} x_{lj}|^2 . \tag{2}$$

For a given field map $\boldsymbol{\omega}$, the ML estimate of $\boldsymbol{x}$ has a closed-form expression [8],[25] that one can substitute into (2) to give the negative log-likelihood in terms of $\boldsymbol{\omega}$:

$$\Phi(\boldsymbol{\omega}) = \min_{\boldsymbol{x}} \widetilde{\Phi}(\boldsymbol{\omega}, \boldsymbol{x}) = \sum_{j=1}^{N_\mathrm{v}} \sum_{m,n=1}^{L} \sum_{c,d=1}^{N_\mathrm{c}} \phi_{cdmnj}(\omega_j) , \tag{3}$$

where

$$\phi_{cdmnj}(\omega_j) \coloneqq |r_{cdmnj}| \big[1 - \cos\left(\angle r_{cdmnj} + \omega_j (t_m - t_n)\right)\big] ,$$

$$r_{cdmnj} \coloneqq \frac{\Gamma_{mn}}{\sum_{c'=1}^{N_\mathrm{c}} |s_{c'j}|^2} s_{cj} s_{dj}^* y_{cmj}^* y_{dnj} , \tag{4}$$

$$\boldsymbol{\Gamma} \coloneqq \boldsymbol{\gamma} (\boldsymbol{\gamma}^* \boldsymbol{\gamma})^{-1} \boldsymbol{\gamma}^* ,$$

where $\cdot^*$ denotes the complex conjugate, and $L \times L$ matrix $\boldsymbol{\Gamma}$ is defined in terms of

$$\boldsymbol{\gamma} = \begin{cases} \mathbf{1} & \text{in field map estimation,} \\ [\mathbf{1} \;\; e^{i2\pi\Delta_\mathrm{f} \boldsymbol{t}}] & \text{in water-fat imaging,} \end{cases} \tag{5}$$

in which $\mathbf{1}$ denotes an all one vector of length L, and the exponential is applied element-wise. In the field map estimation case, this simplifies to $\Gamma_{mn} = 1/L \;\forall\; m, n$.

As B_0 field maps tend to be spatially smooth in MRI, we add a regularization term to (3) to form a penalized-likelihood (PL) cost function

$$\Psi(\boldsymbol{\omega}) = \Phi(\boldsymbol{\omega}) + \frac{\beta}{2} \|\boldsymbol{C}\boldsymbol{\omega}\|_2^2 , \tag{6}$$

where $\boldsymbol{C}$ is a first-order finite difference operator. Such regularization has been used in many prior works [5],[25],[26].

III. Efficient Algorithm

Several approaches have been proposed to solve the field map estimation problem in the single-coil setting, but are demanding in computation or memory. In particular, a quadratic majorizer with a diagonal Hessian [5] takes many iterations to converge even for 2D images, and a quadratic majorizer with an optimal curvature that inverts a $N_\mathrm{v} \times N_\mathrm{v}$ Hessian matrix [25] is memory-limited to small-scale data. In water-fat imaging, [8],[10] process multi-coil data in a coil-wise manner for each voxel, while [9] considers a quadratic majorizer with a diagonal Hessian that also leads to slow convergence.

Here, we optimize (6) using NCG with a MLS [26], and consider a preconditioner with efficient computation and memory storage. Our field map estimation procedure is tabulated in the **Algorithm** below.

For NCG, we choose the Polak-Ribiere update to compute a μ^i that satisfies the conjugacy condition [29].

After estimating the field map $\widehat{\boldsymbol{\omega}}$, we estimate the water and fat components for each voxel in water-fat imaging by applying the closed-form expression [8] using $\widehat{\boldsymbol{\omega}}$:

$$\begin{bmatrix} m_{\mathrm{w},j} \\ m_{\mathrm{f},j} \end{bmatrix} = \Big((\boldsymbol{\gamma} \cdot \operatorname{diag}(e^{i\omega_j \boldsymbol{t}})) \otimes \boldsymbol{s}_j \Big)^\dagger \boldsymbol{y}_j , \tag{7}$$

where $\otimes$ denotes the Kronecker product, $(\cdot)^\dagger$ denotes the pseudo inverse, and $\boldsymbol{s}_j \in \mathbb{C}^{N_\mathrm{c}}$ denotes the coil sensitivity map for the jth voxel.

Next we present our initialization, choice of preconditioner, and derive our iterative monotone line search algorithm in the multi-coil setting.

A. Initialization

For field map estimation, we initialize $\boldsymbol{\omega}$ by the phase difference of the first two acquired images after coil combination, divided by the echo time difference of those two scans:

$$(\omega_j)^0 = \angle \Bigg[\Bigg(\sum_{c=1}^{N_\mathrm{c}} s_{cj}^* y_{c1j} \Bigg)^* \Bigg(\sum_{d=1}^{N_\mathrm{c}} s_{dj}^* y_{d2j} \Bigg) \Bigg] \Big/ (t_2 - t_1) . \tag{8}$$

To initialize $\boldsymbol{\omega}$ for water-fat imaging, we follow [9] and sweep through a range of values from $-|\Delta_\mathrm{f}/2|$ to $|\Delta_\mathrm{f}/2|$ for each voxel, and choose the value with minimal cost (3), denoted as $\widetilde{\boldsymbol{\omega}}^0$. We then run a few CG iterations to minimize a penalized weighted least squares (PWLS) problem

$$\boldsymbol{\omega}^0 = \underset{\boldsymbol{\omega}}{\operatorname{argmin}} \sum_{j=1}^{N_\mathrm{v}} \rho_j (\omega_j - \widetilde{\omega}_j^0)^2 + \frac{\beta}{2} \|\boldsymbol{C}\boldsymbol{\omega}\|_2^2 , \tag{9}$$

Algorithm: Preconditioned NCG-MLS

Inputs:
$\boldsymbol{y}$, $\boldsymbol{s}$, $\boldsymbol{t}$, $\boldsymbol{C}$, β
Intialization:
$\boldsymbol{\omega}^0$ by (8) or (9)
$\boldsymbol{z}^0 = -\nabla\Psi(\boldsymbol{\omega}^0)$
$\alpha^{(0)} = 0$
precompute r_{cdmnj} by (4) and $t_m - t_n$
for $i = 0, 1, \ldots, N-1$ **do**
  compute gradient $\boldsymbol{g}^i = \nabla\Psi(\boldsymbol{\omega}^i)$ with (10)
  precondition $\boldsymbol{p}^i = (\boldsymbol{P}^i)^{-1}\boldsymbol{g}^i$ with (14)
  compute μ^i with conjugacy
  search direction $\boldsymbol{z}^{i+1} = \boldsymbol{p}^i + \mu^i \boldsymbol{z}^i \in \mathbb{R}^{N_\mathrm{v}}$
  for $k = 0, 1, \ldots, N_i - 1$ **do**
    update step size $\alpha^{(k+1)}$ by (17)
  end for
  update $\boldsymbol{\omega}^{i+1} = \boldsymbol{\omega}^i + \alpha^{(N_i)} \boldsymbol{z}^{i+1}$
end for
output: $\boldsymbol{\omega}^N$

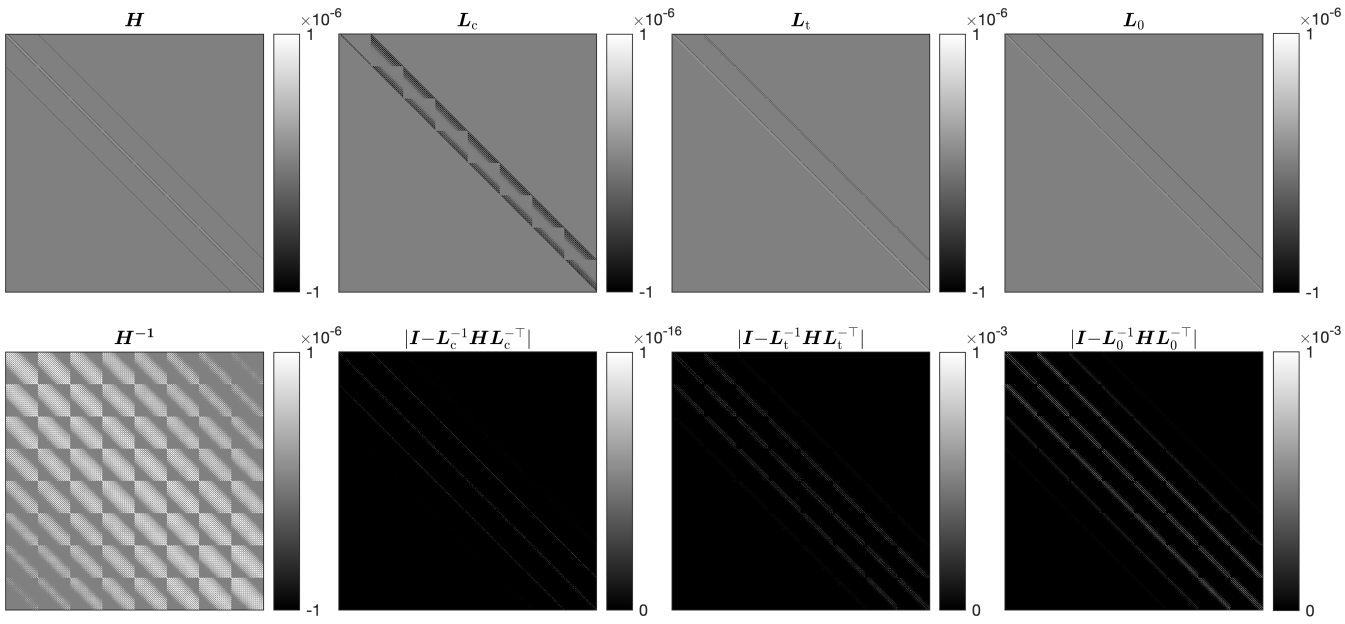

Fig. 1. Matrix structure of each factorization and the error of its inverse, in a toy problem of size $20 \times 16 \times 8$.

where the spatial weights

$$\rho_j = \sum_{m,n=1}^{L} \sum_{c,d=1}^{N_\mathrm{c}} |r_{cdmnj}|$$

are given by (4). We then use $\boldsymbol{\omega}^0$ as our initial estimate in the water-fat case.

B. Preconditioning matrices

To accelerate the NCG-based algorithm, given gradient $\boldsymbol{g}^i$ of the cost at the ith NCG iteration, we explore a preconditioner $\boldsymbol{P}^i$ with memory efficient implementation of $(\boldsymbol{P}^i)^{-1}\boldsymbol{g}^i$ using an incomplete Cholesky factorization [27]. In particular, the gradient $\boldsymbol{g} \in \mathbb{R}^{N_\mathrm{v}}$ is given by

$$\boldsymbol{g} = \nabla\Psi(\boldsymbol{\omega}) = \nabla\Phi(\boldsymbol{\omega}) + \beta \boldsymbol{C}^\top \boldsymbol{C}\boldsymbol{\omega}\,, \tag{10}$$

where

$$\big(\nabla\Phi(\boldsymbol{\omega})\big)_j = \sum_{m,n=1}^{L} \sum_{c,d=1}^{N_\mathrm{c}} |r_{cdmnj}|(t_m - t_n)^2 \cdot \sin\big(\angle r_{cdmnj} + \omega(t_m - t_n)\big)\,.$$

The Hessian of the cost (6) at the ith iteration is the sum of a diagonal matrix and an (approximately, due to the support mask) block Toeplitz with Toeplitz block (BTTB) matrix:

$$\boldsymbol{H}^i = \boldsymbol{D}^i + \beta \boldsymbol{C}^\top \boldsymbol{C} \in \mathbb{R}^{N_\mathrm{v} \times N_\mathrm{v}}\,, \tag{11}$$

where $\boldsymbol{C}$ is the finite difference operation and $\boldsymbol{D}^i = \mathrm{diag}(d_j^i) \succeq 0$, where

$$d_j^i = \sum_{m,n=1}^{L} \sum_{c,d=1}^{N_\mathrm{c}} \kappa_{cdmnj}\big(u_{cdmnj}(\omega_j^i)\big)\,, \tag{12}$$

with

$$\kappa_{cdmnj}(u) = |r_{cdmnj}|(t_m - t_n)^2 \frac{\sin(u)}{u}\,, \text{ and}$$

$$u_{cdmnj}(\omega) = \big(\angle r_{cdmnj} + \omega(t_m - t_n)\big) \bmod \pi\,. \tag{13}$$

Since the terms r_{cdmnj} and $t_m - t_n$ are shared across iterations, we precompute them at the initialization stage to efficiently calculate the gradient and Hessian at each iteration i. Note also that $\boldsymbol{H}^i$ is positive definite as long as at least one value of d_j^i is positive (which is true for any nontrivial problem).

Although $\boldsymbol{H}^i$ is sparse and banded, its inverse is approximately full, so directly computing the inverse would require far too much memory. To reduce memory, we propose a preconditioner that approximates the symmetric Hessian with a LU factorization of the form

$$\boldsymbol{P}^i = \boldsymbol{L}^i (\boldsymbol{L}^i)^\top \approx \boldsymbol{H}^i\,, \tag{14}$$

where $\boldsymbol{L}^i \in \mathbb{R}^{N_\mathrm{v} \times N_\mathrm{v}}$ is sparse lower triangular, enabling efficient computation (via back-substitution) of $(\boldsymbol{P}^i)^{-1}\boldsymbol{g}^i$ in the precondition step. Taking advantage of the sparsity and positive definiteness of our Hessian (11), preconditioning with an incomplete Cholesky factorization reduces both computation and memory. A popular form of the incomplete Cholesky factorization matches the matrix $\boldsymbol{H}$ on its nonzero set, thus is at least as sparse as $\boldsymbol{H}$. In practice, for a better approximation one can control the sparsity by defining a tolerance on the magnitude of the elements, with the trade-off between approximation accuracy and memory storage.

We illustrate the memory improvement by a toy problem of image size $20 \times 16 \times 8$, where we compute $\boldsymbol{H} = \boldsymbol{D} + \beta \boldsymbol{C}^\top \boldsymbol{C}$ and its inverse, with randomly chosen diagonal elements $d_j \in (0, 0.1)$ and $\beta = 0.1$. In Fig. 1, we implement the incomplete Cholesky factorization without tolerance, denoted $\boldsymbol{L}_0$, and with a tolerance of $H_\mathrm{max} \times 10^{-3}$, denoted $\boldsymbol{L}_\mathrm{t}$, where H_max is the element in $\boldsymbol{H}$ with maximum magnitude. Fig. 1 shows the sparse structure of $\boldsymbol{H}$, its nonsparse inverse $\boldsymbol{H}^{-1}$, and the Cholesky factorizations as well as their approximation

	$\boldsymbol{H}$	$\boldsymbol{H}^{-1}$	$\boldsymbol{L}_{\mathrm{c}}$	$\boldsymbol{L}_{\mathrm{t}}$	$\boldsymbol{L}_0$
Number of nonzeros ($\times 10^5$)	1.67	655	72.5	1.77	0.96
Storage (megabytes)	0.31	100.1	11.9	0.53	0.27
NRMSE			3e-16	4e-3	3e-2

Table I. Number of nonzero elements, memory usage, and NRMSE of the inverse of each factorization in a toy problem of size $20 \times 16 \times 8$.

errors. Table I shows the number of nonzero elements of each matrix, their memory storage, and their errors that affect the convergence rate, using the normalized root mean square error (NRMSE) $\|\boldsymbol{I} - \boldsymbol{L}^{-1}\boldsymbol{H}\boldsymbol{L}^{-\top}\|_{\mathrm{F}}/\sqrt{N_{\mathrm{v}}}$ for each factorization $\boldsymbol{L}$ in our example.

For memory storage in this case, the number of nonzero elements in our incomplete Cholesky factor without tolerance $\boldsymbol{L}_0$ is more than 70 times less than that in the (complete) Cholesky factor $\boldsymbol{L}_{\mathrm{c}}$, with more than 40 times of memory saving. In general, we observe (by the banded structures) that the number of nonzero elements of $\boldsymbol{L}_{\mathrm{c}}$ is lower bounded by $(N_{\mathrm{v}} - N_{\mathrm{x}}N_{\mathrm{y}}) * N_{\mathrm{x}}N_{\mathrm{y}}$, while that of $\boldsymbol{L}_0$ is upper bounded by $4N_{\mathrm{v}}$. This leads to the generalization that $\boldsymbol{L}_0$ is at least $(N_{\mathrm{v}} - N_{\mathrm{x}}N_{\mathrm{y}})/(4N_{\mathrm{z}})$ times more sparse than $\boldsymbol{L}_{\mathrm{c}}$, which scales significantly with the problem size. The storage of the incomplete Cholesky factor with tolerance $\boldsymbol{L}_{\mathrm{t}}$ depends on the tolerance, and with the choice of tolerance here we observe a 40 times fewer nonzero values, saving memory by a factor of more than 20 compared with $\boldsymbol{L}_{\mathrm{c}}$.

The trade-off with a sparser factorization, however, is a worst approximation error. This is reflected in the error matrices in Fig. 1 and the NRMSE in Table I. While $\boldsymbol{L}_0$ has lower memory usage than $\boldsymbol{L}_{\mathrm{t}}$, the inverse is a worse approximation to $\boldsymbol{H}^{-1}$. In practice, nevertheless, both incomplete factorizations $\boldsymbol{L}\boldsymbol{L}^{\top}$ are positive definite, so as preconditioners they provide a good descent direction in addition to storage advantage, whereas storing $\boldsymbol{L}_{\mathrm{c}}$ is infeasible for realistically sized 3D datasets.

C. Monotonic step size line search

With a search direction given by NCG, the choice of step size is important for convergence of the algorithm. To avoid multiple function evaluations required by backtracking line search algorithms [30], we implement a recursive line search algorithm using a quadratic majorizer with an optimal curvature, which guarantees monotone decrease of the cost function [31].

In the line search step, given a current field map estimate $\boldsymbol{\omega}^i$ and a search direction $\boldsymbol{z}^i \in \mathbb{R}^{N_{\mathrm{v}}}$, we aim to find a step size that minimizes the cost (6):

$$\widehat{\alpha} = \operatorname*{argmin}_{\alpha} f(\alpha), \text{ where}$$

$$f(\alpha) = \Phi(\boldsymbol{\omega}^i + \alpha\boldsymbol{z}^i) + \frac{\beta}{2}\|\boldsymbol{C}(\boldsymbol{\omega}^i + \alpha\boldsymbol{z}^i)\|_2^2, \qquad (15)$$

We iteratively minimize the nonconvex problem (15) using a quadratic majorizer based on Huber's method [28, p. 184] at the kth inner iteration (dropping outer iteration i for brevity):

$$\begin{aligned} q_k(\alpha) = \Phi(\boldsymbol{\omega} + \alpha^{(k)}\boldsymbol{z}) \\ + \boldsymbol{z}^{\top}\nabla\Phi(\boldsymbol{\omega} + \alpha^{(k)}\boldsymbol{z})(\alpha - \alpha^{(k)}) \\ + \frac{1}{2}d^{(k)}(\alpha - \alpha^{(k)})^2 + \frac{\beta}{2}\|\boldsymbol{C}(\boldsymbol{\omega} + \alpha\boldsymbol{z})\|_2^2, \end{aligned}$$

where the optimal curvature is given by [25]

$$d^{(k)} = \sum_{j=1}^{N_{\mathrm{v}}} |z_j|^2 d_j^{(k)}, \text{where}$$

$$d_j^{(k)} = \sum_{m,n=1}^{L} \sum_{c,d=1}^{N_{\mathrm{c}}} \kappa_{cdmnj}\big(u_{cdmnj}(\omega_j + \alpha^{(k)}z_j)\big), \qquad (16)$$

with $\kappa_{cdmnj}(\cdot)$ and $u_{cdmnj}(\cdot)$ defined in (13).

Using one step of Newton's method on the quadratic majorizer $q_k(\alpha)$ gives the step size update

$$\begin{aligned} \alpha^{(k+1)} &= \alpha^{(k)} - \frac{\frac{\partial}{\partial\alpha}q_k(\alpha^{(k)})}{\frac{\partial^2}{\partial\alpha^2}q_k(\alpha^{(k)})} \\ &= \alpha^{(k)} - \frac{\frac{\partial}{\partial\alpha}f(\alpha^{(k)})}{d^{(k)} + \beta\|\boldsymbol{C}\boldsymbol{z}\|_2^2}. \end{aligned} \qquad (17)$$

We implement (17) efficiently by computing $\|\boldsymbol{C}\boldsymbol{z}\|_2^2$ only once per outer NCG iteration i. Since the majorizer satisfies $q_k(\alpha) \geq f(\alpha)$ for all step size α and inner line search iteration k, the update (17) guarantees monotonic decrease of the cost (15).

IV. Results

We investigated our algorithm and its efficiency with two multi-echo field map estimation experiments and one water-fat imaging experiment, all using 3D parallel MRI data. Due to the large data size, memory intensive methods with a direct solver using the full Hessian are excluded from our experiments. In particular, we compare our incomplete Cholesky preconditioner (NCG-MLS-IC) method versus a quadratic majorizer update with diagonal Hessian (QM) [5] and versus the NCG algorithm without any preconditioner (NCG-MLS) and with a diagonal preconditioner (NCG-MLS-D) [25]. For each dataset, we define a mask using the convex hull of all voxels where the signal is present (with coil-combined image magnitude thresholded below by $0.1y_{\mathrm{max}}$, where y_{max} denotes the maximum image magnitude in the coil-combined image for the first echo time.), with a dilation of two voxels. We then computed $\boldsymbol{\omega}$ within the mask, and tuned the regularization parameter β by sweeping across a range of values. To compare their convergence, we computed the root mean square difference (RMSD) to an $\boldsymbol{\omega}^{\infty}$ that averages the estimates of two methods with fastest convergence. All our experiments used MATLAB R2020a, with a 2.4-GHz dual-core Intel Core i7. The MATLAB code that reproduces the experiments with our efficient algorithm will be available as part of the Michigan Image Reconstruction Toolbox (MIRT) [32].

A. Brain Simulation

We first simulated a 3D brain dataset with 40 64×64 slices, 4 simulated coils and 3 echo times $t_l = 0, 2, 10$ ms, with added complex Gaussian noise so that the SNR ≈ 20 dB. To generate multi-coil data, we simulated coil sensitivity maps with 4 coils based on [33] using the MIRT. We set $\beta = 2^{-3}$ as our regularization parameter to achieve visual resemblance to the ground truth field map. In light of the trade-off between storage and approximation error discussed in Section III-B, we explored preconditioners using the incomplete Cholesky factorization both without tolerance (NCG-MLS-IC-0) and with a tolerance of $H^i_{\max} \times 10^{-3}$ for each iteration i (NCG-MLS-IC).

Fig. 2 shows four selected slices, their initial field map, and the regularized estimate by our algorithm. To examine the speed of convergence, we plot the RMSD $\|\boldsymbol{\omega}^i - \boldsymbol{\omega}^\infty\|_2/\sqrt{N_{\mathrm{v}}}$ versus wall time. The RMSD plots in Fig. 3 show significant computational gain of NCG-MLS preconditioned with the incomplete Cholesky factorization over using quadratic majorizer or NCG-MLS without and with a diagonal preconditioner. We observe that using a tolerance in the incomplete Cholesky factorization gives a faster convergence than not using one, hence we adopt that choice for the NCG-MLS-IC implementations in our next experiments.

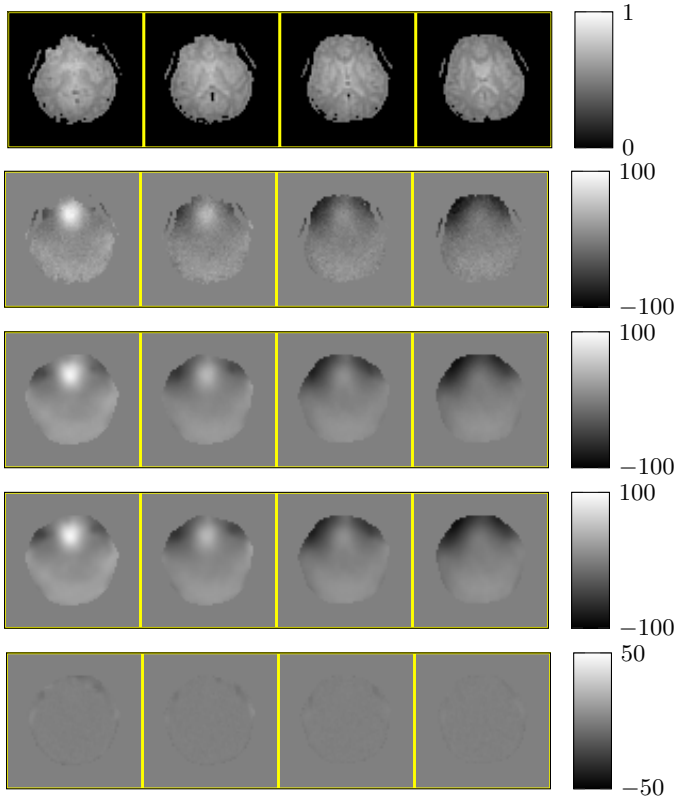

Fig. 2. Top to bottom: selected slices of coil-combined simulation image, initial field map (in Hz), regularized field map estimate $\widehat{\boldsymbol{\omega}}$, ground truth field map $\boldsymbol{\omega}_{\text{true}}$, and error $|\widehat{\boldsymbol{\omega}} - \boldsymbol{\omega}_{\text{true}}|$.

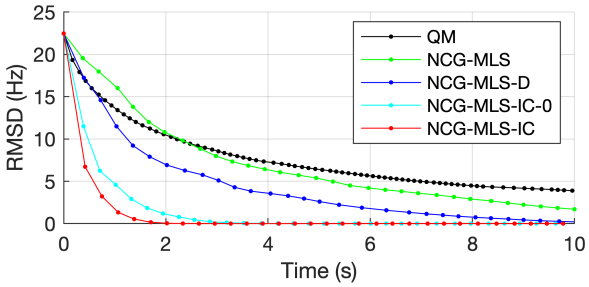

Fig. 3. RMSD of four algorithms used in simulation. Every iteration is marked by a dot.

B. Phantom Dataset

Our second experiment uses a Function Biomedical Informatics Research Network (FBIRN) phantom [34] with two pieces of metal staple to induce field inhomogeneity, collected on a GE MR750 3T scanner with a 32-channel Nova Head Coil receiver. This dataset has size $74 \times 74 \times 10$ with 3 mm^3 isotropic voxel size, TR = 10.5 ms, with 3 echo times $t_l = 0, 1, 2.3$ ms. We computed coil sensitivity maps using ESPIRiT [35], and set $\beta = 2^{-3}$ as in the simulation.

Fig. 4 shows four selected slices, their initial field map, and the regularized estimate by our algorithm. The RMSD

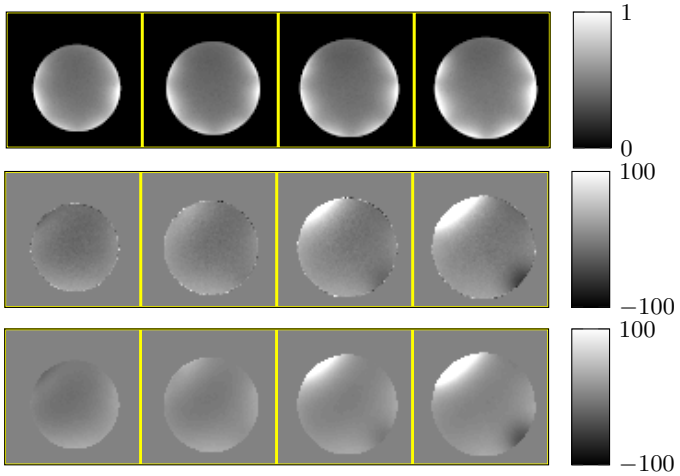

Fig. 4. Top to bottom: selected slices of coil-combined phantom image, initial field map (in Hz), and regularized field map estimate.

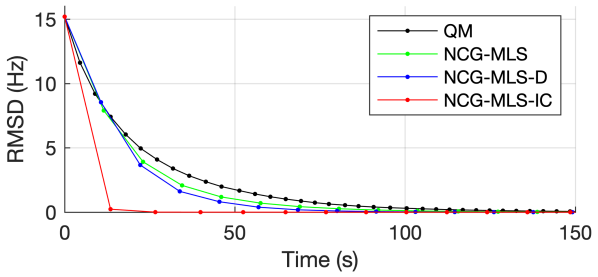

Fig. 5. RMSD of four algorithms used in the phantom experiment. Every iteration is marked by a dot.

	QM	NCG-MLS	NCG-MLS-D	NCG-MLS-IC
Time (s)	96	81	69	4.5
vs. IC time	21×	18×	15×	

Table II. Time for each method to reach an RMSD below 0.5 Hz, and their relative proportions to the time taken by NCG-MLS-IC.

plots in Fig. 5 show that our algorithm again converges much faster than the other three, reaching 0.33 Hz RMSD in 1 iteration, and 0.005 Hz RMSD in 2 iterations. Since this 3D dataset has a more realistic problem size than the simulated data, we quantify the convergence speedup by comparing the time it takes for each method to reach an RMSD below 0.5 Hz. Table II shows that our NCG-MLS algorithm with an incomplete Cholesky preconditioner provides a 15 times speedup from NCG-MLS with a diagonal preconditioner, 18 times from that without a preconditioner, and 21 times from the quadratic majorizer implementation.

C. Ankle Water-Fat Dataset

For water-fat imaging, we used 3D multi-coil ankle scans from the ISMRM Fat-Water Separation Dataset [36]. This dataset has 4 256×256 slices, 8 coils and 3 echo times $t_l = 2.2, 3, 3.8$ ms, in a 3T scanner that corresponds to $\Delta_{\mathrm{f}} \approx 440$ Hz. We chose $\beta = 2^{-10}$ as our regularization parameter to achieve visual separation of water and fat components.

Fig. 6 shows the 1st echo image, the initial field map $\widetilde{\boldsymbol{\omega}}^0$ by voxel-wise estimation, and the initial $\boldsymbol{\omega}^0$ after 10 CG iterations of PWLS minimization (9), and the regularized estimate by our algorithm. For completeness, Fig. 6 also shows the estimated water and fat images using (7), which achieve a visual separation of the two components. However, it is worth emphasizing that our main interest is in the speed of finding a minimizer of the problem (6). The RMSD plots in Fig. 7 show a significant computational gain of our algorithm over the other algorithms.

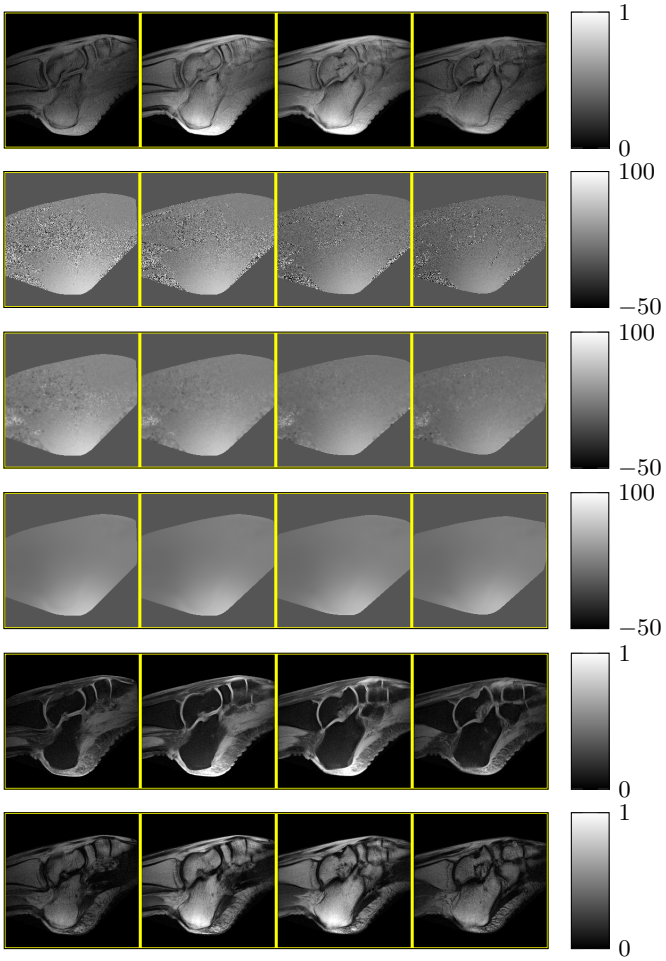

Fig. 6. Top to bottom: coil-combined water-fat simulation image for the 1st echo, initial field map $\widetilde{\boldsymbol{\omega}}^0$ (in Hz) by voxel-wise estimation, initial fieldmap $\boldsymbol{\omega}^0$ by PWLS (9), regularized field map estimate, estimated water image, and estimated fat image.

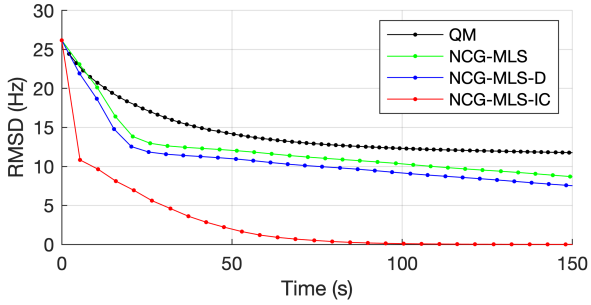

Fig. 7. RMSD of four algorithms used in the water-fat experiment. Every iteration is marked by a dot.

V. Conclusion

This paper presents an efficient algorithm for both multi-echo field map estimation and water-fat imaging problem in the 3D parallel MRI setting. Given the nonconvex cost function, our algorithm uses the nonlinear conjugate gradient method with a preconditioner based on a incomplete Cholesky factorization, and a monotonic step size line search based on a quadratic majorizer with optimal curvatures. This is the first work to use the incomplete Cholesky factorization as a preconditioner for multi-coil field map estimation. Experiments with simulation and phantom data show that our method has faster convergence than existing memory-efficient methods that use quadratic majorizers or with a diagonal preconditioner.

Acknowledgement

We thank Jon-Fredrik Nielsen at the University of Michigan for the multi-echo 3D parallel MRI phantom data.

References

[1] K. Sekihara, S. Matsui, and H. Kohno, "NMR imaging for magnets with large nonuniformities," *IEEE Trans. Med. Imag.*, vol. 4, no. 4, pp. 193–199, 1985.

[2] P. Jezzard and R. S. Balaban, "Correction for geometric distortion in echo planar images from B0 field variations," *Mag. Res. Med*, vol. 34, no. 1, pp. 65–73, 1995.

[3] P. J. Reber, E. C. Wong, R. B. Buxton, and L. R. Frank, "Correction of off resonance-related distortion in echo-planar imaging using EPI-based field maps," *Mag. Res. Med*, vol. 39, no. 2, pp. 328–330, 1998.

[4] D. C. Noll, J. A. Fessler, Jeffrey A, and B. P. Sutton, "Conjugate phase MRI reconstruction with spatially variant sample density correction," *IEEE Trans. Med. Imag.*, vol. 24, no. 3, pp. 325–336, 2005.

[5] A. K. Funai, J. A. Fessler, D. T. B. Yeo, V. T. Olafsson, and D. C. Noll, "Regularized field map estimation in MRI," *IEEE Trans. Med. Imag.*, vol. 27, no. 10, pp. 1484–1494, 2008.

[6] G. H. Glover and E. Schneider, "Three-point Dixon technique for true water/fat decomposition with B0 inhomogeneity correction," *Mag. Res. Med.*, vol. 18, no. 2, pp. 371–383, 1991.

[7] S. B. Reeder, Z. Wen, H. Yu, A. R. Pineda, G. E. Gold, M. Markl, and N. J. Pelc, "Multicoil Dixon chemical species separation with an iterative least-squares estimation method," *Mag. Res. Med.*, vol. 51, no. 1, pp. 35–

45, 2004.

[8] D. Hernando, Diego, J. P. Haldar, B. P. Sutton, J. Ma, P. Kellman, and Z-P. Liang, "Robust water/fat separation in the presence of large field inhomogeneities using a graph cut algorithm," *Mag. Res. Med*, vol. 59, no. 3, pp. 571–580, 2008.

[9] W. Huh, J. A. Fessler, and A. A. Samsonov, "Water-fat decomposition with regularized field map," *in Proc. Intl. Soc. Mag. Res. Med.*, 2008, p. 1382.

[10] D. Hernando, P. Kellman, J. P. Haldar, and Z-P. Liang, "Robust water/fat separation in the presence of large field inhomogeneities using a graph cut algorithm," *Mag. Res. Med*, vol. 63, no. 1, pp. 79–90, 2010.

[11] T. A. Bley, O. Wieben, C. J. Franois, J. H. Brittain, and S. B. Reeder, "Fat and water magnetic resonance imaging," *J. Mag. Res. Im.*, vol. 31, no. 1, pp. 4–18, 2010.

[12] S. B. Reeder, A. R. Pineda, Z. Wen, A. Shimakawa, H. Yu, J. H. Brittain, G. E. Gold, C. H. Beaulieu, and N. J. Pelc, "Iterative decomposition of water and fat with echo asymmetry and least-squares estimation (IDEAL): Application with fast spin-echo imaging," *Mag. Res. Med*, vol. 54, no. 3, pp. 636–644, 2005.

[13] H. Yu, S. B. Reeder, A. Shimakawa, J. H. Brittain, and N. J. Pelc, "Field map estimation with a region growing scheme for iterative 3-point water-fat decomposition," *Mag. Res. Med*, vol. 54, no. 4, pp. 1032–1039, 2005.

[14] W. Lu and B. A. Hargreaves "Multiresolution field map estimation using golden section search for water-fat separation," *Mag. Res. Med*, vol. 60, no. 1, pp. 236–144, 2008.

[15] M. Jacob and B. P. Sutton, "Algebraic decomposition of fat and water in MRI," *IEEE Trans. Med. Imag.*, vol. 28, no. 2, pp. 173–184, 2009.

[16] K. Zhou, M. Zaitsev, and S. Bao, "Reliable two-dimensional phase unwrapping method using region growing and local linear estimation," *Mag. Res. Med*, vol. 62, no. 4, pp. 1085–1090, 2009.

[17] M. Doneva, P. Börnert, H. Eggers, A. Mertins, J. Pauly, and M. Lustig, "Compressed sensing for chemical shift-based waterfat separation," *Mag. Res. Med*, vol. 64, no. 6, pp. 1749–1759, 2010.

[18] C. Windischberger, S. Robinson, A. Rauscher, M. Barth, and E. Moser, "Robust field map generation using a triple-echo acquisition," *J. Mag. Res. Im.*, vol. 20, no. 4, pp. 730–734, 2004.

[19] E. Schneider and G. Glover "Rapid in vivo proton shimming," *Mag. Res. Med*, vol. 18, no. 2, pp. 335–347, 1991.

[20] P. Irarrazabal, C. H. Meyer, D. G. Nishimura, and A. Macovski, "Inhomogeneity correction using an estimated linear field map," *Mag. Res. Med*, vol. 35, no. 2, pp. 278–282, 1996.

[21] S. D. Sharma, H. H. Hu, and K. S. Nayak, "Chemical shift encoded water-fat separation using parallel imaging and compressed sensing," *Mag. Res. Med*, vol. 69, no. 2, pp. 456–466, 2013.

[22] S. D. Sharma, H. H. Hu, and K. S. Nayak, "Accelerated water-fat imaging using restricted subspace field map estimation and compressed sensing," *Mag. Res. Med*, vol. 67, no. 3, pp. 650–659, 2012.

[23] J. Tsao and Y. Jiang "Hierarchical IDEAL: Fast, robust, and multiresolution separation of multiple chemical species from multiple echo times," *Mag. Res. Med*, vol. 70, no. 1, pp. 155–159, 2013.

[24] J. M. Bioucas-Dias and G. Valado, "Phase unwrapping via graph cuts," *IEEE Trans. Imag. Proc.*, vol. 16, no. 3, pp. 698–709, 2007.

[25] M. J. Allison and J. A. Fessler, "Accelerated computation of regularized field map estimates," *in Proc. Intl. Soc. Mag. Res. Med.*, 2012, p. 0413.

[26] G. Ongie, J. Shi, and J. A. Fessler, "Efficient computation of regularized field map estimates in 3D," *IEEE ISBI*, pp. 700–703, 2017.

[27] T. A. Manteuffel, "An incomplete factorization technique for positive definite linear systems," *Mathematics of Computation*, vol. 34, no. 150, pp. 473–97, 1980.

[28] P. J. Huber, "Robust Statistics," New York: Wiley, 1981.

[29] E. Polak and G. Ribierer, "Note sur la convergence de méthodes de directions conjuguées," *ESAIM*, vol. 3, no. R1, pp. 35–43, 1969.

[30] J. Nocedal and S. Wright, "Efficient computation of regularized field map estimates in 3D," *Numerical optimization*, 2006.

[31] J. A. Fessler and S. D. Booth, "Conjugate-gradient preconditioning methods for shift-variant PET image reconstruction," *IEEE Trans. Imag. Proc.*, vol. 8, no. 5, pp. 688–699, 1999.

[32] "Michigan Image Reconstruction Toolbox (MIRT)," http://web.eecs.umich.edu/~fessler/code, [Online; accessed 20-Feb.-2020].

[33] M. I. Grivich and D. P. Jackson, "The magnetic field of current-carrying polygons: An application of vector field rotations," *American J. Phys.*, vol. 68, no. 5, pp. 469–474, 2000.

[34] D. B. Keator *et al.*, "The function biomedical informatics research network data repository," *Neuroimage*, vol. 124, pp. 1074–1079, 2016.

[35] M. Uecker, P. Lai, M. J. Murphy, P. Virtue, M. Elad, J. M. Pauly, S. S. Vasanawala, and M. Lustig, "ESPIRiT an eigenvalue approach to autocalibrating parallel MRI: where SENSE meets GRAPPA," *Mag. Res. Med.*, vol. 71, pp. 990–1001, 2014.

[36] "Fat-Water Toolbox," http://ismrm.org/workshops/FatWater12/data.htm, [Online; accessed 7-March-2020].